

Influence of the coordination defects on the dynamics and the potential energy landscape of two-dimensional silica

Projesh Kumar Roy^{1, 2, 3} and Andreas Heuer^{4, a)}

¹⁾*The Institute of Mathematical Sciences, C.I.T. Campus, Taramani, Chennai 600113*

²⁾*Homi Bhabha National Institute, Training School Complex, Anushakti Nagar, Mumbai 400094, India*

³⁾*NRW Graduate School of Chemistry, Wilhelm-Klemm-Straße 10, 48149 Münster, Germany*

⁴⁾*Institute für Physikalische Chemie, Westfälische-Wilhelms-Universität Münster, Corrensstraße 28/30, 48149 Münster, Germany*

(*Electronic mail: andheuer@uni-muenster.de)

(Dated: 2 August 2022)

The main cause of the fragile-to-strong crossover of 3D silica was previously attributed to the presence of a low-energy cutoff in the potential energy landscape. The important question emerges about the microscopic origin of this crossover and the generalizability to other glass-formers. In this work, the fragile-to-strong crossover of a model 2D glassy system is analyzed via molecular dynamics simulation, which represents 2D-silica. By separating the sampled defect and defect-free inherent structures, we are able to identify their respective density of states distributions with respect to energy. A low energy cutoff is found in both distributions. It is shown that the fragile-to-strong crossover can be quantitatively related to the parameters of the energy landscape, involving in particular the low-energy cutoff of the energy distribution. It is also shown that the low-energy cutoff of the defect-states is determined by the formation energy of a specific defect configuration, involving two silicon and no oxygen defect. The low-temperature behavior of 2D silica is quantitatively compared with that of 3D silica, showing surprisingly similar behavior.

Keywords: Silica co-ordination defects, Fragile to strong crossover, Two-dimensional silica

I. INTRODUCTION

The origin of the anomalous temperature dependence of viscosity is a matter of debate for glassy systems. In general, the dynamical behavior of the glassy systems can be described either as ‘Strong’ or ‘Fragile’, depending on the nature of the relationship between the viscosity (η) and temperature (T); i.e. the Angell plot¹ ($\ln(\eta(T))$ vs β , where $\beta = 1/K_B T$). Assuming the validity of the Stokes-Einstein relation², one can represent $\eta(T) \propto 1/D(T)$, where $D(T)$ represents the diffusivity of the fluid. The strong glasses obey the Arrhenius-type temperature dependence of the diffusion constant, i.e. $D(T) \propto \exp(-\beta V_0)$, where V_0 is the average activation energy of the fluid. In contrast, the dynamics of the fragile glasses are usually described with the empirical Vogel-Fulcher-Tammann (VFT) equation³⁻⁶

$$D(T) \propto \exp\left(\frac{\alpha}{T - T_0}\right) \quad (1)$$

where α , and T_0 are empirical constants. Experimentally, it has been shown that, several compounds undergo a Fragile-to-Strong crossover (FSC) at a certain temperature range⁷⁻¹³, which is usually close to the glass transition temperature. Interestingly, molecules with tetrahedral ordering show a general tendency for such behavior in the bulk state¹³⁻¹⁶. The fragile behavior of glasses at high temperatures—i.e. the power-law behavior of the relaxation time—can be explained

with the help of mode-coupling theory^{17,18}. Upon cooling, the transition to Arrhenius behavior is often correlated with a supposed liquid-liquid phase transition, which generally occurs in the super-cooled region¹⁹⁻²⁴. However, a proper physical mechanism for FSC—at either bulk or molecular level—is not well understood. Potential energy landscape (PEL) analysis of the glassy systems provides a good understanding of the FSC phenomenon at low temperatures. It is known that, below the mode-coupling temperature, the dynamics and the thermodynamics of the system start to correlate, and the nature of the dynamical properties strongly reflect the properties of the PEL. In this region, the nature of the PEL can be described by the properties of the underlying minima, i.e. Inherent States (IS)²⁵⁻³². At higher temperatures, the fragile behavior can be linked to the multiplicity and the width of the underlying IS-energy distributions^{33,34}. With decreasing temperature, the configurational entropy of the system (S_c) decreases, and the widths of the basins in the PEL landscape become narrower. Following the Adam-Gibbs theory³⁵, one can determine the relaxation time and subsequently the diffusivity as a function of the S_c in the low-temperature region as $D(T) \propto \exp(-B/TS_c)$, where B is a constant. Therefore, if S_c is independent of temperature³⁶⁻³⁸, a transition from fragile to strong behavior can be related to an inflection in S_c . Using molecular dynamics simulations, Saksengwijit et al.³⁹ had shown that in case of BKS-silica⁴⁰, there exists a cutoff in the density of states (DOS) distribution of IS’s at a certain energy. The presence of such a cutoff prevents S_c from vanishing at low temperatures and thus avoids the Kauzmann paradox. However, determination of the nature of reduction of S_c at low temperature is a difficult task in simulation as it is computationally demanding^{41,42}. Thus, proper calculation of the FSC

^{a)}<https://www.uni-muenster.de/Chemie.pc/en/forschung/heuer/index.html>

temperature from the IS analysis remains challenging.

The microscopic origin of FSC varies from system to system. Poly-amorphism³⁸ was often suspected to be the drive behind the FSC phenomenon. For example, a two-state model was proposed by Tanaka et al.^{43–45} to explain the viscosity anomaly of water. In this model, two different configurations of *locally favored* small clusters of water molecules controls the bulk properties of water. The FSC in water can thus be explained from the population ratio of such clusters, both of which separately follow Arrhenius type temperature dependence of viscosity. This model predicts a smooth crossover from the fragile to the strong regime, and was able to predict the crossover temperature, T_{FSC} , quite well^{44,45}. In case of several tetrahedrally ordered halide-molecules¹³; e.g. ZnCl_2 ^{12,46}, BeF_2 ^{10,46}, GeSe_2 ^{47–49}; the reduction of the S_c near FSC has also been correlated to the changes in the ordering of the local environment. For these materials, in both experiment^{12,46,49} and simulation^{50,51}, a sharp change has been observed in the ratio of the local edge-sharing tetrahedral ordering to entropically favored corner-sharing tetrahedral ordering, with lowering temperature in the vicinity of FSC. These results clearly indicate that FSC is linked to the specific microscopic environment of the fluid. Recently a continuum model, in conjugation to the two-state theory, is proposed to explain the non-Arrhenius behavior of the liquids using non-linear Fokker-Plank equations^{52,53}.

Despite the similarity between the molecular structure (tetrahedral) of water and silica, they exhibit several differences in terms of cluster formation⁵⁴. While the structure of the water-clusters are controlled by the hydrogen-bond network, silica-clusters are controlled by the flexibility of the bridging-oxygen bonds. As a result, although water and silica exhibits some dynamical and thermodynamical similarity—e.g. density anomaly, FSC, etc.—their microscopic origin can be somewhat different. Saksangwitt et al.³⁹ had postulated that for BKS-silica⁴⁰, the FSC can be related to a decrease in the fraction of coordination defects. As the temperature of the system is lowered, the fraction of the coordination defects in silica decreases. Recently, using replica exchange molecular dynamics, Yu et al.⁴¹ have shown that the rate of such a decrease shows a sharp increase near its fictive temperature. Thus, near the cutoff, one can postulate that the defect states would completely disappear. This, in turn, should result in an arrest in the hopping dynamics of silica as the effective activation energy for the bond-breaking process would be very large^{39,55}.

In this paper, we study the FSC behavior of a 2D model system which represents an allotrope of silica, namely the two-dimensional silica⁵⁶ (2D-silica). This material is an ideal member to study the properties of a natural glass forming system with computer simulation since an atomistic scale description of the real structure is available directly from the experiment. 2D-silica is grown on Ru⁵⁷ or Graphene surfaces⁵⁸ via vapor deposition and in-situ oxidation. The binding of 2D-silica with the underlying surface is quite weak which makes it a free-standing material⁵⁹. However, the material is extremely thin with a height of just ~ 3 atoms in the Z-direction⁵⁷. Therefore, measuring high temperature properties

of this material is quite difficult as it would desorb from the surface during heating. Thus, for this system the FSC behavior is expected to be inaccessible via experiments. Therefore, computer simulations play an important role to elucidate the properties of this system close to the FSC.

The objective of this paper is to show that the PEL description of the dynamical behavior works well for the description of FSC in the 2D-silica model. Similar to the BKS-silica model, we aim to correlate the presence of a cutoff in the PEL with the FSC phenomenon in 2D-silica. We provide further insight into the microscopic environment of 2D-silica near the FSC in terms of the coordination defects. The paper is organized as follows. We start with a short account of the methods in section II and analyze the density of states (DOS) distributions. In section III, we study the changes in the PEL influenced by the coordination defects and explicitly show that the FSC is related to the cutoff in the PEL. Afterwards, we show in section IV that a specific local arrangement of the particles is present at the low energy limit which is independent of the system size, thus yielding insight into the structural and energetic properties of the defects. We finish with a conclusion and outlook.

II. METHODS

A. Simulation

In our previous works^{60–62}, we have used a Yukawa type force-field to describe the structural and thermodynamical properties of 2D-silica in close similarity with the experimental results, which reads

$$V_{ij}(r_{ij}) = \left[\left(\frac{\sigma_{ij}}{r_{ij}} \right)^{12} + \left(\frac{q_{ij}}{r_{ij}} \right) \exp(-\kappa r_{ij}) \right] \quad (2)$$

For details of the simulation parameters, we refer to the reference 60. With a 80 particle system in a square box of side length 19.67 Å, we performed a molecular dynamics simulation under NVT conditions for a wide range of temperatures using Nosé-Hoover chains thermostat^{63,64}, and an elementary timestep of 0.01. We sample the inherent structures and their energies (E_{IS}) by quenching the trajectory with a frequency of 100 steps. Except for the mean square displacement (MSD) calculations, we use the minimized structures for analysis throughout the paper.

B. Defects

In our analysis, we separate the IS's based on the coordination defects. We denote an IS as a defect-free-state (abbreviation: df), if all Si particles have 3 O particles and all O particles have 2 Si particles within an empirical cutoff distance of 2.0 Å. Otherwise the IS is termed as defect-state (abbreviation: d). The choice of this cutoff is based on the $g_{\text{Si-O}}(r)$ analysis⁶⁰, which showed a sharp peak around 1.5-1.6 Å at

the low energy regime. Since we are interested in the structural features of the model at low temperatures, the choice of the distance cutoff is sufficient in identifying any coordination defects in the structure.

C. Reweighting

With the sampled IS structures at one given temperature, one can calculate the DOS ($G(E_{\text{IS}})$) at different energies. This calculation is performed by binning the distribution of inherent structures $P(E_{\text{IS}}, T)$ and reweighting the resulting energy distribution with an inverse Boltzmann factor, i.e.

$$G(E_{\text{IS}}) \propto P(E_{\text{IS}}, T)e^{\beta E_{\text{IS}}} \quad (3)$$

Naturally, one unknown energy-independent proportionality constant remains. Similarly, one can define $G_{\text{d}}(E_{\text{IS}})$ and $G_{\text{df}}(E_{\text{IS}})$ as the DOS of the defect-states and defect-free-states, respectively. We note that this relation, i.e. the estimation of a temperature independent DOS, is valid as long as anharmonic effects in the vibrations within an IS are not too strong^{32,65}. Strictly speaking the DOS should be rather interpreted as an effective DOS because each state is also weighted by the harmonic partition function, i.e. by the inverse square root of the frequency³². It is known that the DOS distribution of a binary Lennard-Jones liquid or BKS-silica has a Gaussian shape over a large energy range^{65–67}.

To determine $G(E_{\text{IS}})$ over a broad energy range, based on the Boltzmann distributions from different temperatures, one could try to overlap the different $G(E_{\text{IS}})$ -curves, obtained from different temperatures. A procedure to obtain the DOS in a statistically optimized way is the Weighted Histogram Analysis Method (WHAM)⁶⁸. To obtain the DOS $G(E_{\text{IS}})$ we use the algorithm developed by Gallicchio *et al.*⁶⁹ which reads for the present application

$$G(E_{\text{IS}}) = \frac{\sum_i N(E_{\text{IS}}, T_i)}{\sum_i N_i(T_i) f_i(T_i) c_i(E_{\text{IS}}, T_i)} \quad (4)$$

Here, $N(E_{\text{IS}}, T_i)$ is the total counts of the states at energy bin E_{IS} at temperature T_i and $N(T_i) = \sum_j N(E_{\text{IS}}^j, T_i)$. $c_i(E_{\text{IS}}, T_i)$ is called a component of the *biasing matrix*, which is calculated as

$$c_i(E_{\text{IS}}, T_i) = \exp[-\beta_i E_{\text{IS}}]$$

From there, one can optimize the normalization factor $f_i(T_i)$ as

$$f_i^{-1}(T_i) = \sum_j c_i(E_{\text{IS}}^j, T_i) G(E_{\text{IS}}^j, T_i)$$

We iteratively optimize the normalization factor $f_i(T_i)$ until convergence is reached and the DOS can be read off. Note that

the resulting DOS is defined except for one proportionality constant.

In analogy this procedure can be applied as well for the determination of $G_{\text{d}}(E_{\text{IS}})$ and $G_{\text{df}}(E_{\text{IS}})$. However, due to the unknown proportionality constants we would not be able to determine, e.g., the fraction of defect-free-states $q_{\text{df}}(E_{\text{IS}})$ at a given energy E_{IS} . Naturally, from equilibrium simulations at a given temperature T_i one can directly read off this fraction $q_{\text{df}}^i(E_{\text{IS}}, T_i)$. Since this fraction is an equilibrium property, in the limit of infinite sampling it would not depend on temperature. In the spirit of WHAM we join the information from the simulations at the different temperatures for the estimation of $q_{\text{df}}(E_{\text{IS}})$ via

$$q_{\text{df}}(E_{\text{IS}}) = \frac{\sum_i N(E_{\text{IS}}, T_i) q_{\text{df}}^i(E_{\text{IS}}, T_i)}{\sum_i N(E_{\text{IS}}, T_i)} \quad (5)$$

In practice we first determine $G(E_{\text{IS}})$ (via WHAM) and $q_{\text{df}}(E_{\text{IS}})$ as described above and then estimate the DOS for the defect-free-states and defect-states, respectively, via

$$\begin{aligned} G_{\text{df}}(E_{\text{IS}}) &= G(E_{\text{IS}}) q_{\text{df}}(E_{\text{IS}}) \\ G_{\text{d}}(E_{\text{IS}}) &= G(E_{\text{IS}}) (1 - q_{\text{df}}(E_{\text{IS}})) \end{aligned} \quad (6)$$

III. PEL PROPERTIES AND THEIR RELATION TO THE DIFFUSIVITY

In this section, we investigate the DOS distributions of defect and defect-free states with energy using the WHAM optimized energy distributions in the previous section. All important parameters, to be discussed below, are summarized in Table I.

TABLE I. Values of the important variables used in section III. For the description of the variables, see main text and supporting material (SM).

| | |
|---|--------|
| $E_{\text{df}}^{\text{cutoff}}$ (Figure 1(c)) | -27.04 |
| $E_{\text{d}}^{\text{cutoff}}$ (Figure 1(c)) | -26.93 |
| E_0^{cross} (Figure 1(c)) | -26.86 |
| $E_{\text{IS}}^{\text{max}}$ (Figure SM.1(a)) | -25.77 |
| $E_{\text{d}}^{\text{max}}$ (Figure 1(b)) | -25.89 |
| $E_{\text{df}}^{\text{max}}$ (Figure 1(c)) | -26.56 |
| s_{IS} (Figure SM.1(a)) | 0.12 |
| s_{d} (Figure 1(b)) | 0.12 |
| s_{df} (Figure 1(c)) | 0.07 |
| V_0 (Figure 2(a)) | 0.26 |

A. Density of states

In Figure 1(a) we show the Boltzmann distribution $p_{\text{d}}(E_{\text{IS}}, T)$ of defect-states for a large range of temperatures. Whereas for the highest temperature (curve at the right end) the distribution is basically Gaussian, one observes for lower temperatures deviations from the Gaussian shape in the low-energy range and the presence of a cutoff-energy of $E_{\text{d}}^{\text{cutoff}} = -26.93$. This value does not seem to depend on temperature.

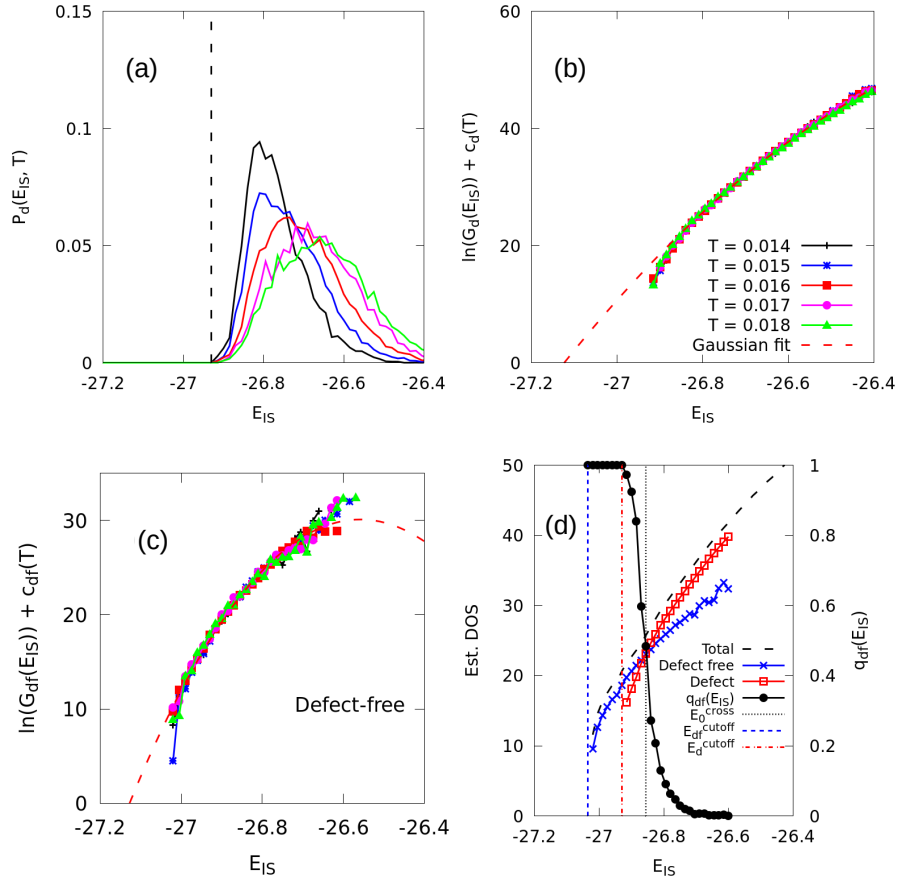


FIG. 1. (a) The plot for the normalized Boltzmann distributions of the defect-states for temperatures between $T=0.014$ and $T=0.018$. One can estimate the cutoff energies for the defect-states at ~ -26.93 . (b) DOS of defect-states, obtained from the data in (a) via Boltzmann reweighting. The data at $T=0.015$ are fitted with a Gaussian function $\ln G(E) = -\frac{1}{2}[(E - E_d^{\max})/s]^2 + c_d(T)$ with $E_d^{\max} = -25.89$, $s_d = 0.12$ and an arbitrary shift parameters $c_d(T)$. (c) DOS of defect-free states, obtained in a similar way as (b) with $E_{df}^{\max} = -26.56$, $s_{df} = 0.07$. (d) The plot for the estimated DOS from the WHAM analysis for defect-states, defect-free-states, and all states. The total DOS curve (marked as *Total*) is slightly shifted along the Y-axis for better visual inspection. The fraction of defect-free states at each energy level ($q_{df}(E_{IS})$) is also shown and its values are related to the right Y-axis. For a complete list of different parameters, see Table I.

In the next step, we reconstructed the underlying DOS via simple reweighting (see Figure 1(b)). Indeed, we find that over a large range of energies DOS curves overlap with each other, which confirmed that the simulations at the lowest temperatures have been done at equilibrium. Similar observation can be made for the total DOS and the defect-free DOS as well (see supporting material, Figure SM.1). In the high energy range, the DOS seems to depend on temperature. As mentioned above, this indicates the presence of significant anharmonic effects for high temperatures. For a large range of energies the distribution follows a Gaussian shape. Importantly, in the low-energy range the DOS of defect-states decays much faster than a Gaussian distribution, reflecting the presence of the cutoff-energy. The analogous results for the defect-free-states are shown in Figure 1(c) (see also supporting material Figure SM.1(a), for DOS of all-states). Finally, in Figure 1(d) we show the results of the WHAM analysis, i.e. the DOS $G(E_{IS})$, $G_d(E_{IS})$, $G_{df}(E_{IS})$, as well as the fraction of defect-free-states $q_{df}(E_{IS})$. Note that the relevant energy

regime, shown in this figure, only covers the regime where the determination of the DOS is not hampered by anharmonic effects. Also for the defect-free-states we find a low-energy cutoff. The estimated cutoff energy of the defect-free-states, $E_{df}^{\text{cutoff}} \approx -27.04$ is significantly lower than E_d^{cutoff} , namely $\Delta E^{\text{cutoff}} = E_d^{\text{cutoff}} - E_{df}^{\text{cutoff}} \sim 0.11$. As a consequence, also the overall DOS $G(E_{IS})$ displays the same cutoff as $G_d(E_{IS})$. Such a cutoff-energy was also observed in case of BKS-silica³⁹.

Interestingly, ΔE^{cutoff} hardly changes when increasing the system size from 80 to 200 particles ($\Delta E^{\text{cutoff}}(N=200) \sim 0.12$ as can be derived from the data in supporting material Figure SM.2). This result suggests that the minimal number of particles, required to create a defect state, is independent of size. Later we will show that the structure of the defect-states at the cutoff energy involves a well-defined local environment, other than the usual trigonal geometry so that the energy of 0.11 can be interpreted as a minimum defect formation energy. Furthermore, E_{df}^{cutoff}/N hardly varies with system size.

Thus the energy of the lowest energy state, which is a defect-free state, is an extensive property. Due to the local character of the formation of a defect it is expected that E_d^{cutoff} is not extensive. This is indeed clearly seen in supporting material Figure SM.2.

Finally, we discuss the properties of the fraction of defect-free-states $q_{\text{df}}(E_{\text{IS}})$. It has an asymmetric behavior: whereas at low energies one observes a sharp cutoff, below which only defect-free-states are available, at high temperatures there is a more gradual approach towards the limit where only defect-states are present. Indeed, as seen from the supporting material (Figure SM.1), there is no indication of a strict cutoff-energy at high energies, although defect-free-states become exponentially rare. Nevertheless, there is a fast transition from the energy regime governed by defect-free-states to the regime governed by defect-states. In fact, it takes an energy variation of less than 0.06 to change between $q_{\text{df}}(E_{\text{IS}}) = 0.2$ and $q_{\text{df}}(E_{\text{IS}}) = 0.8$. The crossover energy, E_0^{cross} , where $q_{\text{df}}(E_{\text{IS}}) = 0.5$, i.e. where the number of defect-free-states and defect-states is identical, turns out to be -26.86. In terms of per-particle energies, the value of E_0^{cross} gets lower for a larger system size, see the supporting material (Figure SM.2). This is because the probability of finding defect-free-states decreases exponentially with increasing system size⁶⁰. This is a consequence of the fact that a large system can be decomposed into approximately independent smaller subsystems. Then it becomes very unlikely that the total system contains no defect because this requires that every subsystem is defect-free. This underlines the importance of studying a smaller system sizes where the statistical characterization of defect-free-states is far easier.

B. Fragile to strong crossover

Next we explore a possible relation between the kinetics and the thermodynamics of the system. In Figure 2(a) we show the temperature-dependent diffusion constant. One clearly finds a transition from non-Arrhenius to simple Arrhenius behavior,

$$D(T) = D_0 \exp[-V_0\beta], \quad (7)$$

i.e. a transition from fragile to strong behavior. We have added fits with the VFT equation in the high-temperature and an Arrhenius fit in the low-temperature regime. Starting from the VFT fit, the first significant deviation is seen for $\beta \approx 80$.

To relate the kinetics to the thermodynamics of the system, we provide the average IS energy ($E_{\text{IS}}^{\text{av}}(T)$) in Figure 2(b). Again, two temperature regimes can be observed. Both have a simple interpretation. If the DOS is governed by a Gaussian distribution with variance s^2 one expects a linear behavior

$$E_{\text{IS}}^{\text{av}}(T) = E_{\text{IS}}^{\text{max}} - \beta s^2. \quad (8)$$

Indeed, this is seen in the high-temperature regime in Figure 2(b). The negative slope of 0.013 is very close to the result of the Gaussian fit ($s^2 = 0.014$), reported in Table I. Naturally,

in the low-temperature regime the average energy starts to approach the cutoff-energy. Most importantly, the impact of the cutoff-energy again starts to be visible around $\beta \approx 80$ which is exactly the same temperature regime as observed for the FSC. This strongly suggests a direct causal relation between the kinetics and the thermodynamics. We mention in passing that the crossover temperature can be estimated from the condition $E_{\text{IS}}^{\text{av}}(T) \approx E_{\text{df}}^{\text{cutoff}} + s$. The second summand expresses the fact that the energy-cutoff starts to matter as soon as the cutoff is within a standard deviation to the average energy (in Gaussian approximation). Using the values $s = 0.12$, $E_{\text{IS}}^{\text{max}} = -25.77$ (see supporting material, Figure SM.1), and $E_{\text{df}}^{\text{cutoff}} = -27.04$, one obtains $\beta = 79.8$ which is basically identical to the estimated crossover temperature of $\beta \approx 80$.

C. Comparison with bulk silica

A similar behavior has been previously observed for standard 3D bulk silica, simulated with the standard BKS force field³⁹. For that system the causality could be directly proven⁵⁵. Here we may compare some numbers in order to see similarities and differences between 2D silica and 3D silica. However, before starting we estimate the crossover temperature for 3D ($s = 3.5$ eV, $E_{\text{IS}}^{\text{max}} = -1867$ eV, and $E_{\text{df}}^{\text{cutoff}} = -1910.7$ eV) as $T = 0.30$ eV \approx 3500 K which agrees very well with the emergence of the crossover behavior of the diffusivity and the average energy, reported in reference 39.

- (i) *System size*: For the estimation of the diffusivity one can define an energy-dependent activation energy $E_{\text{eff}}(E_{\text{IS}})$ ⁵⁵ which for 3D silica can be written to a very good approximation as (for $E_{\text{IS}} \geq E_{\text{df}}^{\text{cutoff}}$)

$$E_{\text{eff}}(E_{\text{IS}}) \approx \lambda (E_{\text{df}}^{\text{cutoff}} - E_{\text{IS}}) + V_0 (E_{\text{df}}^{\text{cutoff}}). \quad (9)$$

More generally, the possibility to formulate a relation between activation energy and IS energy (strictly speaking metabasin energy, which, however, for the typically visited IS at low temperatures is basically identical) shows the generally strong connection between the dynamic properties and the nature of the PEL for glass-forming systems^{30,65,70,71}. The value $\lambda \leq 1$ has a simple interpretation: $\lambda \times N$ is the size of the hypothetical elementary subsystem to which relaxation processes are basically confined. Indeed it has been shown³² that by doubling the system size the value of λ decreases by a factor of 2. From the data in reference 55 one can estimate $\lambda \approx 0.6$. Thus, for the system size of $N = 99$, used for the simulation of bulk silica, an elementary system comprises approx. 60 particles.

For the present case we have no direct information for the estimation of λ . However, we can formulate an upper bound. Naturally, for the highest temperature where anharmonic effects do not matter ($\beta \approx 60$) one still has activated behavior, i.e. $E_{\text{eff}}(E_{\text{IS}}^{\text{av}}(\beta = 60)) \gtrsim 0$. This implies (using $V_0(E_{\text{df}}^{\text{cutoff}}) = 0.26$, see Figure 2(a), and

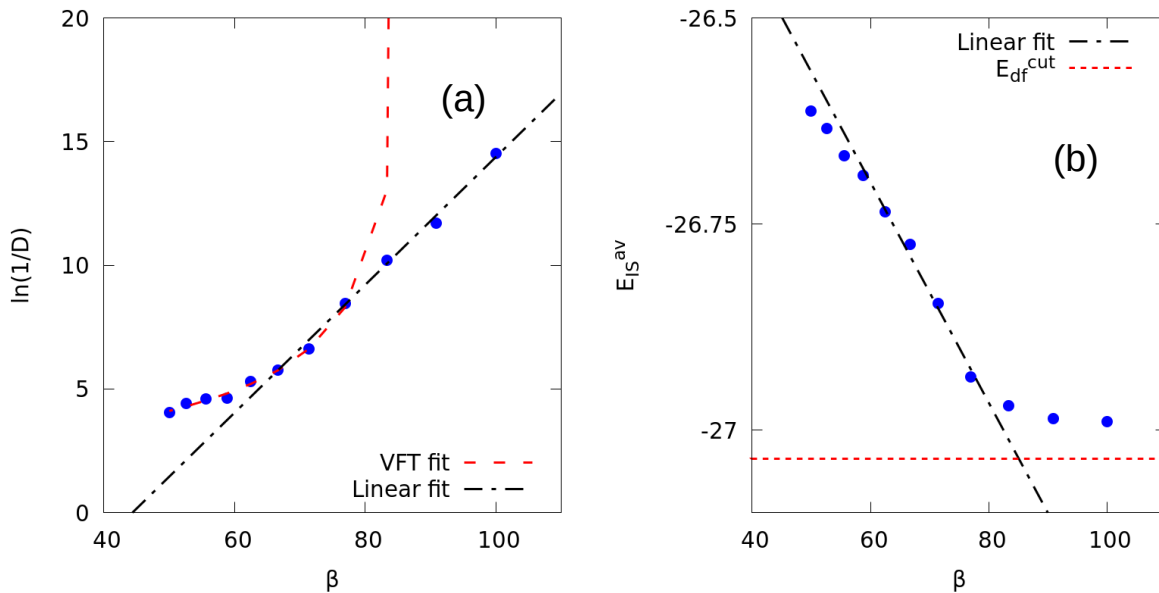


FIG. 2. (a) Dependence of $\ln(1/D)$ on inverse temperature. The data are fitted with the VFT equation (equation 1) for $\beta < 77$ and with an Arrhenius equation, i.e. $T_0 = 0$, for $\beta \geq 77$. Values of α , and T_0 are ≈ 0.01 , and 0.011 , respectively. The value of V_0 is 0.26 . (b) Dependence of the average energy on inverse temperature. A linear fit is performed between $62.5 \leq \beta \leq 77$ with slope ~ -0.013 . The cutoff energy for the total system, which is the same as for the defect-free-states (E_{df}^{cut}), is also shown as a horizontal line.

$E_{IS}^{av}(\beta = 60) = -26.69$ that $\lambda \leq 0.74$. Thus, the hypothetical elementary subsystem has a size of less than $0.74 \times 80 \approx 60$ particles.

- (ii) *PEL landscape*: A natural dimensionless number, characterizing the shape of the DOS, is given by $[E_{IS}^{max} - E_{df}^{cutoff}]/s$. It expresses the impact of the cutoff-energy relative to the overall shape of the Gaussian. In the present case we have $(-25.77 + 27.04)/0.12 = 10.6$. Reading off the corresponding values for bulk silica from reference 39, we obtain $(-1867 \text{ eV} + 1910.7 \text{ eV})/3.5 \text{ eV} = 12.5$. However, for a direct comparison we need to take into account that these ratios depend on system size. Whereas the energies in the numerator scale with the system size, the standard deviation in the denominator scales with the square root of the system size. For a fair comparison the values should be evaluated for the respective elementary system sizes. However, that with the present data it cannot be excluded that the elementary system sizes are comparable, the same holds for the shape of the DOS.

- (iii) *Defect-states vs. defect-free-states*: One may ask for the energy to generate defects. In the present case it is given by $\Delta E^{cutoff} \approx 0.11$. To obtain an appropriate dimensionless number we may relate this value to the crossover temperature, yielding $(0.11/(1/80)) \approx 8.8$. Interestingly, for bulk silica there exist defect-states very close to the cutoff-energy of defect-free-states. From the data in reference 39 one may estimate $\Delta E_{3D}^{cutoff} \approx 1.0 \text{ eV}$. This yields a ratio of $(1 \text{ eV}/0.3 \text{ eV}) = 3.3$ which is significantly smaller than 8.8. One may

speculate that in 3D there exist more degrees of freedom so that defects with (relatively) lower energy costs can be generated.

- (iv) *Activation energy*: We represent activation energy as a ratio of the low-temperature activation energy to the crossover temperature, which makes it a dimensionless number and independent of the system size. Whereas for the 2D system we have a ratio of $(0.26/(1/80)) \approx 21$, the corresponding ratio for the 3D system reads (data taken from reference 39) $(4.84 \text{ eV} / 0.30 \text{ eV}) \approx 16$. Thus, the effective barriers for the relaxation processes agree relatively well. The remaining differences may be related to a similar argument as in (iii) that in 3D there are more degrees of freedom which allow the system to explore more energy-efficient paths.

IV. STRUCTURAL ASPECTS

A. Ring statistics

We start by studying the statistics of ring sizes as a function of energy. In Figure 3(a) we show the standard deviation of the ring distribution. As expected in thermodynamic equilibrium, at given energy the standard deviation does not depend on temperature within statistical uncertainties. One observes a different dependence on energy when crossing the crossover energy E_0^{cross} . A more detailed perspective is shown in Figure 3(b). It turns out that with increasing temperature, the probability of finding 5, 6, and 7 rings decreases, whereas for all other rings it increases. It is an expected behavior, since

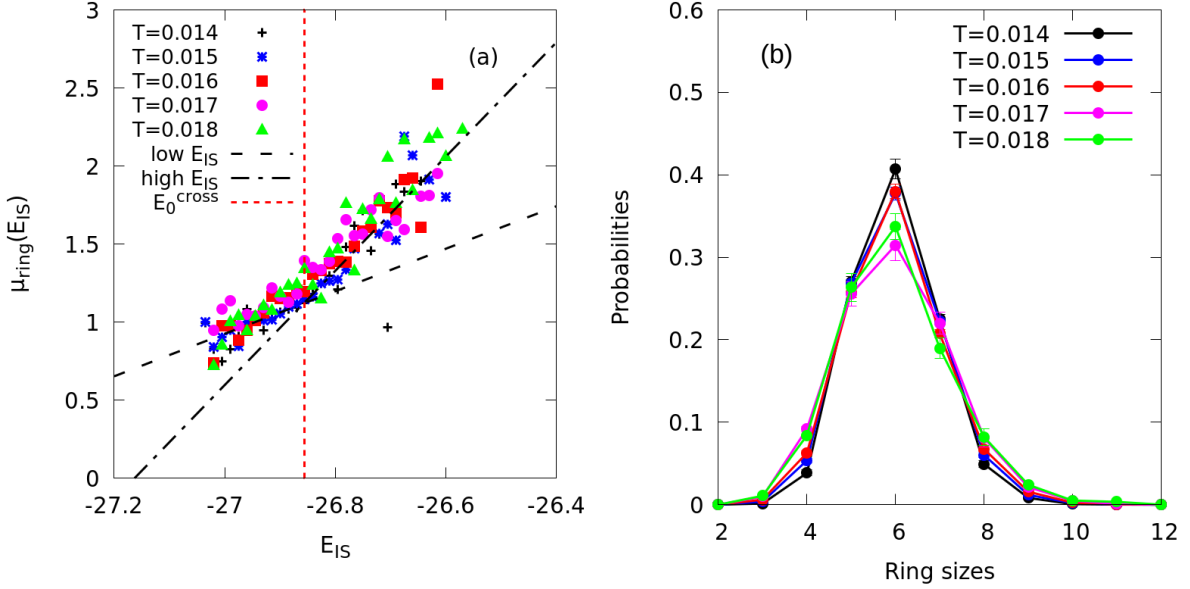


FIG. 3. (a): Dependence of the standard deviation of the ring distribution (μ_{ring}) with energy for defect-free-states. Data below E_0^{cross} and above E_0^{cross} at $T = 0.015$ are fitted separately with a line. (b): Probability distribution of the ring-sizes at various temperatures.

large ($>$ ringsize 7) and small ($<$ ringsize 5) rings are quite strained and hence have higher energies^{61,62}.

B. Energy-dependent defect properties

To examine the properties of the defect-states in the low-energy limit, we sort the defect-states according to the number of *defect-Si* particles, denoted d_{Si} . Here, we do not distinguish whether a defect-Si particle has more or less than 3 O neighbors. The probabilities to find a specific number of defect-Si particles at a given energy are shown in Figure 4(a). Clearly, the silicon defect states exactly disappear at E_d^{cutoff} . Again, the data are obtained from averaging over all temperatures, in analogy to Equation 5. Actually, the average number of defect-Si particles linearly increases with energy above E_d^{cutoff} (see supporting material, Figure SM.3). Similar to the observation of Yu et al⁴¹ in BKS-silica, we find that the slope of the number of defect particles vs. energy decreases with increasing energy. After excluding $d_{Si} = 0$ states, the appropriately renormalized data are shown in Figure 5(a). We find that very close to E_d^{cutoff} , all defect-states have two silicon defects, i.e. $d_{Si} = 2$. In particular, there are no defect states with just one silicon defect. They only start to appear at slightly higher energies. This is also reflected in the anomalous behavior of the average number of defects (excluding $d_{Si} = 0$ states), shown in the supporting material Figure SM.3.

Analogously, we study the properties of oxygen defects. In Figure 4(b), the probabilities to find a specific number of defect-O particles are shown. We find that already above E_d^{cutoff} no oxygen defects are present. Thus, there exists an energy range where two silicon defects are present but no oxygen defect (see below for a closer characterization of that

state). For states slightly above E_d^{cutoff} , in average two defect-Si but no defect-O particles are present.

The structures of the $d_{Si} = 2$ defect states are further analyzed by counting different Si-O co-ordinations (C_{Si-O}) of the participating defect-Si particles (i, j), such as, $C_{Si-O}^i = 1$ and $C_{Si-O}^j = 4$ (abbreviation: 1-4 defect); ($C_{Si-O}^i = 2$ and $C_{Si-O}^j = 2$ (abbreviation: 2-2 defect); $C_{Si-O}^i = 2$ and $C_{Si-O}^j = 4$ (abbreviation: 2-4 defect). As shown in Figure 5(b), near E_d^{cutoff} only 2-4 defect states are observed. Performing a similar analysis for $d_{Si} = 1$ states, we find that only $C_{Si-O} = 2$ co-ordination is present for the single defect-Si particle at all energies. We find that such a Si-O co-ordination for $d_{Si} = 1$ states is not possible with $d_O = 0$ but with $d_O = 1$, as by definition co-ordination numbers of the Si and O particles are dependent on each other. Performing a similar co-ordination number analysis to only $d_O = 1$ states, we find that corresponding C_{O-Si} is strictly 1 within our simulation set up.

Next, we analyze the spatial correlations in between the defect-Si particles in each frame by calculating the average distance between them in dependence of energy, $r_{defect}(E_{IS})$. The results are shown in Figure 6. We find that the minimum value is $\langle r_{defect}(E_{IS}) \rangle \sim 3 \text{ \AA}$, which is also the average distance between two Si particles in a defect-free state⁶⁰. The average distance between the defect particles increases with energy and becomes constant after a certain energy range, suggesting that a breakdown of any spatial correlations among defect-Si particles. The limiting value of the average distance can be calculated by evaluating the integral,

$$\frac{L}{2} \int_0^1 dx \int_0^1 dy \sqrt{x^2 + y^2} \sim 0.77 \frac{L}{2} \quad (10)$$

which for the 80 particle system corresponds to ~ 7.55 .

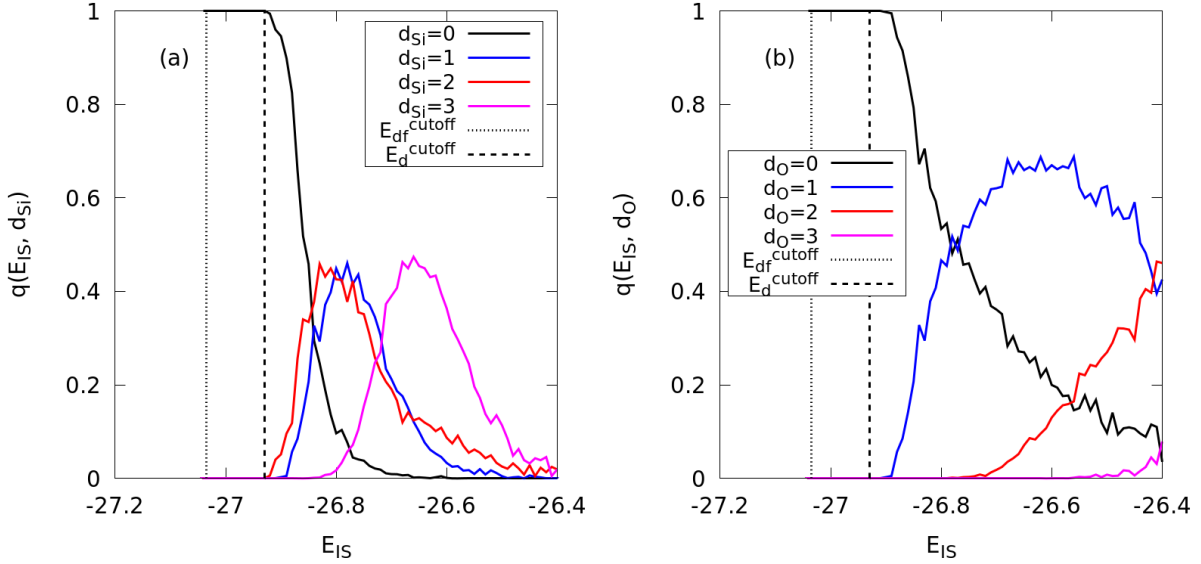


FIG. 4. (a): Probability $q(E_{IS}, d_{Si})$ to find a specific defect state with d_{Si} number of average defect-Si particles at energy E_{IS} . (b): Probability $q(E_{IS}, d_O)$ to find a specific defect state with d_O number of average defect-O particles at energy E_{IS} .

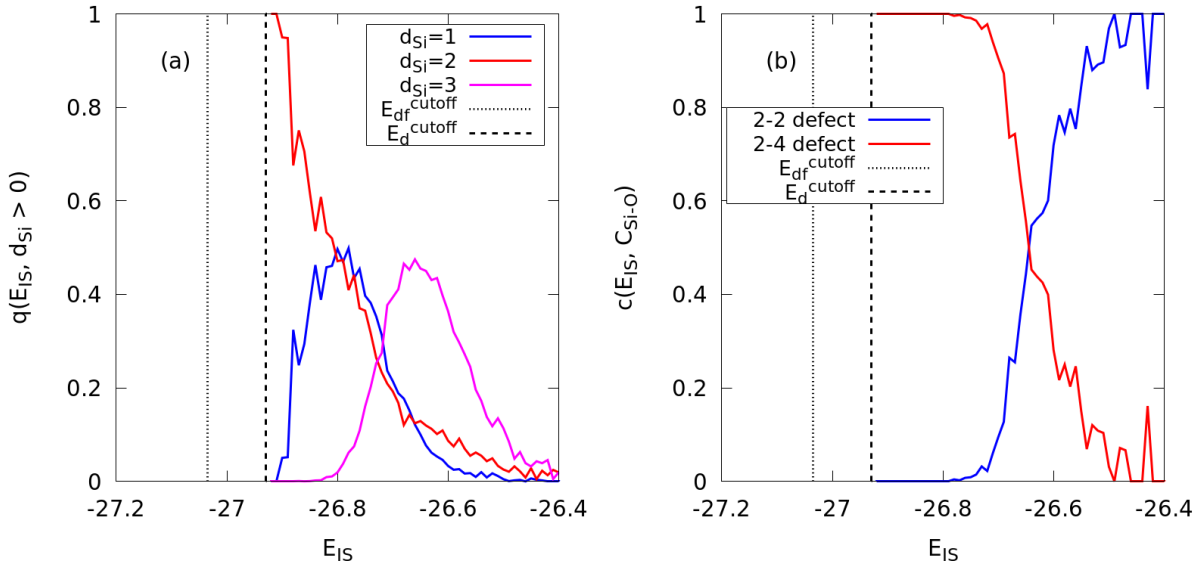


FIG. 5. (a) Probability $q(E_{IS}, d_{Si} > 0)$ to find a specific defect state with d_{Si} number of average defect-Si particles at energy E_{IS} , excluding $d_{Si} = 0$ states. (b) Probability $c(E_{IS}, C_{Si-O})$ to find a specific combination of the co-ordinations of the defect-Si particles for $d_{Si} = 2$ states at energy E_{IS} , normalized by the total number of $d_{Si} = 2$ states. 1-4 defects are ignored in this plot due to very small probability.

C. Microscopic realizations

These results suggest that there exists a locally well-defined defect structure for the defect-states close to E_d^{cutoff} . This structure involves no defect-O particles but two close-by defect-Si particles within a distance of $\sim 3 \text{ \AA}$. The two defect-Si particles have a coordination number of 2 and 4, respectively, yielding the average co-ordination numbers $\langle C_{Si-O} \rangle =$

3, $\langle C_{O-Si} \rangle = 2$ for the total system at E_d^{cutoff} .

A typical structure of the $d_{Si} = 2$ states close to the E_d^{cutoff} is shown in Figure 7(a). Starting from a defect-free structure, one can generate this defect-structure by transferring one O particle from one Si particle to an adjacent Si particle. With increasing energy, more O particles are transferred further along the network and the average distance between defect-Si particles ($\langle r_{defect} \rangle$) increases from 3 \AA . This result has a trivial size dependence, as the oxygen transfer can hap-

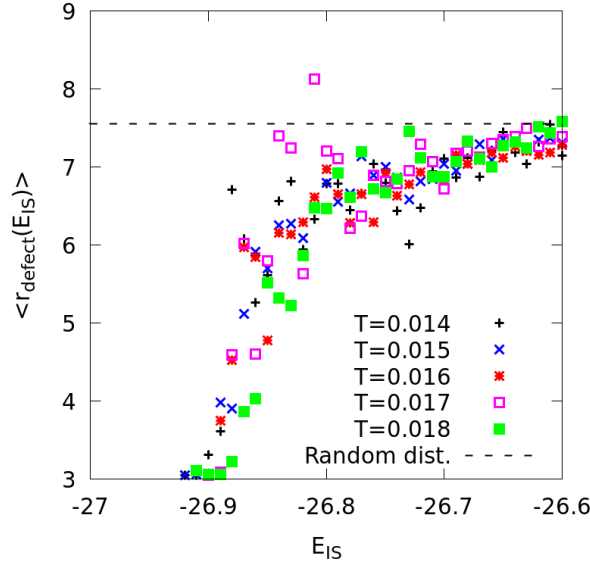


FIG. 6. Average distance between two defect-Si particles. The limit of a random distribution is shown at $\langle r_{\text{defect}}(E_{\text{IS}}) \rangle \sim 7.55$.

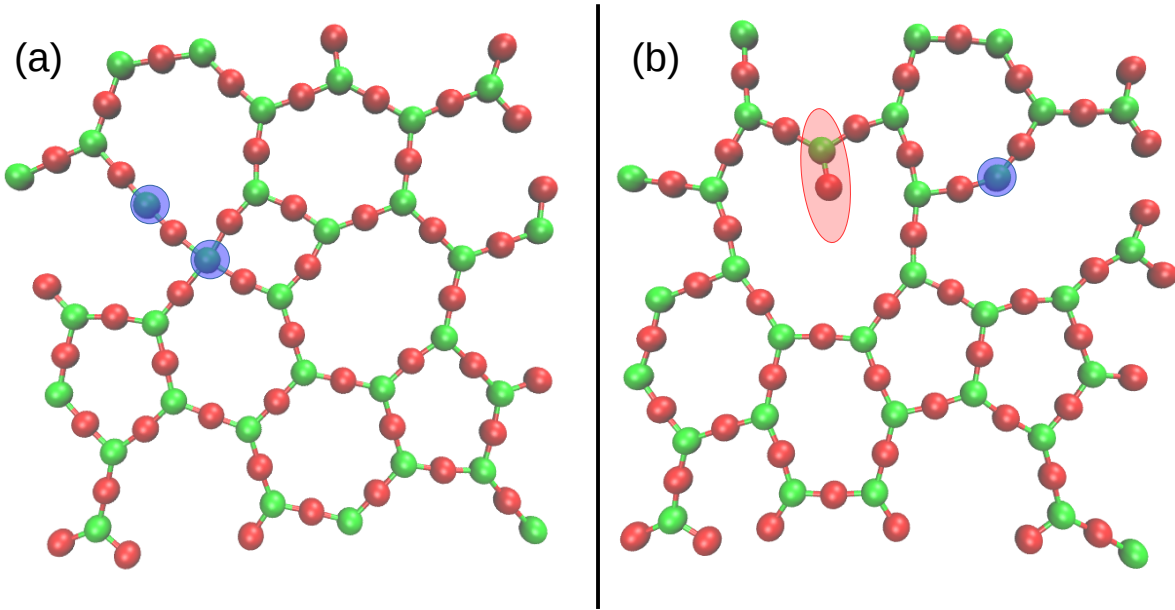


FIG. 7. Sample structures for states with (a) 2 defect Si particles and (b) 1 defect Si particle. The defect Si particles are marked in blue. The dangling Si-O bond in (b) is marked with a red ellipse.

pen simultaneously at larger distances. As a result, the value of $\langle r_{\text{defect}} \rangle$ in Figure 6 may increase at low energies for large systems. This again underlines the need to study small systems to clearly elucidate the energy-dependent structural properties at low energies. Furthermore, it explains our observation that the difference between the two cutoff energies ΔE^{cutoff} is practically independent of system size.

A typical state with $d_{\text{Si}} = 1$ is displayed in Figure 7(b). These structures involve a dangling O particle with coordination number 1. Comparison of the states with $d_{\text{Si}} = 2$ and $d_{\text{Si}} = 1$ suggest that from an energetic point of view a state

with $d_{\text{Si}} = 2$ is closer to the defect-free states than $d_{\text{Si}} = 1$ and thus has the chance to display a lower energy.

The result shows that the average number of defect particles and average co-ordination number of the system may not have a linear relationship with energy, at least near $E_{\text{d}}^{\text{cutoff}}$. Indeed, as shown in the supporting material Figure SM.4(a), the average co-ordination number of defect-Si states (excluding $d_{\text{Si}} = 0$ states) shows a minimum, roughly around the same location where $d_{\text{Si}} = 1$ states are most populated. This effect can be attributed to the lower $\langle C_{\text{Si-O}} \rangle$ value of $d_{\text{Si}} = 1$ states as compared to the $d_{\text{Si}} = 2$ states. Interestingly, we find

that for defect-O states (excluding $d_O = 0$ states), the average co-ordination number is constant to 1 throughout the relevant energy range within our simulation set up. The relatively late appearance of $d_O = 2,3$ states in the energy spectrum might be a reason for this observation.

V. CONCLUSION AND OUTLOOK

In this work, we have shown that the phenomenon of FSC in 2D-silica model can be directly related to the properties of the PEL. We find that the both defect and defect-free-states have a low energy cutoff. The energy difference between these energies does not depend on system size which is a first hint that the low-energy defect-states are fully local. Similar to the case of BKS-silica, we find that at the temperature where the system senses the presence of the final low-energy cutoff, the fragile to strong crossover (FSC) in the kinetics is observed. The results suggest that the emergence of the low-energy cutoff of $G_{\text{dr}}(E_{\text{IS}})$ (or $G(E_{\text{IS}})$) is the major cause of the FSC.

Structurally, the properties of the low-energy defect states have been clearly characterized. One can see that the defect ground-state is a spatially coupled pair of defect-Si particles which does not involve any dangling bond, in contrast to a structure with just a single defect-Si particle. Thus the absence of a dangling bond renders the double defect structure energetically more favorable.

The quantitative comparison between the 2D and 3D silica system showed strong similarities. A minor difference is given by the observation that the low-temperature activation energy for the 2D system is approx. 30% higher than for the 3D system. This may be related to the difficulty in the 2D system to find reaction coordinates with low energy barriers. Furthermore, we would like to stress that the 2D activation energy is more than twice as high as the energy difference of the overall ground-state and the ground-state defect structure (0.26 vs. 0.11). This reflects the complexity which is involved in the transition between two defect-free states, dominating at low temperatures, as well as the additional impact of activation barriers.

The present analysis has again shown that the choice of small system sizes is essential to learn about specific PEL-related properties. Otherwise the low-energy properties would be smeared out and it would be difficult to identify the microscopic origin of the FSC beyond the mere identification of similar crossover temperatures in the thermodynamic and kinetic properties.

It will be interesting to use a three-body force-field (like Stillinger-Weber potential⁷²) in addition to the two-body Yukawa force-field, and analyze how the new 2D-silica model changes its properties near the FSC-regime. In the present 2D-silica model, it is possible to unambiguously separate defect and defect-free-states based on a single cutoff radius at all temperatures. It remains to be seen if similar analysis can be performed in other network forming materials which show FSC as well, such as water.

SUPPLEMENTARY MATERIAL

See supplementary material for (i) DOS curves for defect, defect-free, and total IS distributions; (ii) DOS curves for 80-particle and 200-particle systems; (iii) Average number of defect Si/O particles with energy; (iv) Average co-ordination number with energy.

ACKNOWLEDGMENTS

The authors thank the NRW Graduate School of Chemistry and the University of Münster for providing necessary funding.

AUTHOR DECLARATIONS

Conflict of Interest

There are no conflicts of interests to declare.

Author Contributions

Andreas Heuer: Funding acquisition, project planning, and supervision. **Projesh Kumar Roy:** Simulation and data creation. Both authors contributed equally in writing the manuscript.

DATA AVAILABILITY

The data that support the findings of this study are available within the article and its supplementary material.

- ¹C. A. Angell, *Journal of Non-Crystalline Solids* **131-133**, 13 (1991).
- ²A. Einstein, *Ann. Physik* **19**, 371 (1906).
- ³H. Vogel, *Phys. Z.* **22**, 645 (1921).
- ⁴G. S. Fulcher, *Journal of the American Ceramic Society* **8**, 339 (1925).
- ⁵G. Tamman and W. Hesse, *Z. Anorg. Allg. Chem.* **156**, 245 (1926).
- ⁶G. W. Scherer, *Journal of the American Ceramic Society* **75**, 1060 (1992).
- ⁷C. A. Angell, *Annual Review of Physical Chemistry* **34**, 593 (1983).
- ⁸C. A. Angell, *Science* **267**, 1924 (1995).
- ⁹K.-U. Hess, D. Dingwell, and E. R  ssler, *Chemical Geology* **128**, 155 (1996), 5TH Silicate Melt Workshop.
- ¹⁰M. Hemmati, C. T. Moynihan, and C. A. Angell, *The Journal of Chemical Physics* **115**, 6663 (2001).
- ¹¹E. F. Riebling, *The Journal of Chemical Physics* **43**, 499 (1965).
- ¹²P. Lucas, G. J. Coleman, M. Venkateswara Rao, A. N. Edwards, C. Devaadhithya, S. Wei, A. Q. Alsayoud, B. G. Potter, K. Muralidharan, and P. A. Deymier, *The Journal of Physical Chemistry B* **121**, 11210 (2017), pMID: 29166015.
- ¹³P. Lucas, *Journal of Non-Crystalline Solids: X* **4**, 100034 (2019).
- ¹⁴R. Shi and H. Tanaka, *Proceedings of the National Academy of Sciences* **115**, 1980 (2018).
- ¹⁵J. Russo, K. Akahane, and H. Tanaka, *Proceedings of the National Academy of Sciences* **115**, E3333 (2018).
- ¹⁶R. Shi and H. Tanaka, *Science Advances* **5**, 10.1126/sciadv.aav3194 (2019).
- ¹⁷M. De Marzio, G. Camisasca, M. Rovere, and P. Gallo, *The Journal of Chemical Physics* **144**, 074503 (2016).
- ¹⁸F. W. Starr, F. Sciortino, and H. E. Stanley, *Phys. Rev. E* **60**, 6757 (1999).

- ¹⁹L. Xu, P. Kumar, S. V. Buldyrev, S.-H. Chen, P. H. Poole, F. Sciortino, and H. E. Stanley, Proceedings of the National Academy of Sciences **102**, 16558 (2005).
- ²⁰P. H. Poole, F. Sciortino, U. Essmann, and H. E. Stanley, Nature **360**, 324 (1992).
- ²¹O. Mishima and H. E. Stanley, Nature **396**, 329 (1998).
- ²²J. C. Palmer, F. Martelli, Y. Liu, R. Car, A. Z. Panagiotopoulos, and P. G. Debenedetti, Nature **510**, 385 (2014).
- ²³P. H. Poole, F. Sciortino, U. Essmann, and H. E. Stanley, Phys. Rev. E **48**, 3799 (1993).
- ²⁴P. H. Poole, U. Essmann, F. Sciortino, and H. E. Stanley, Phys. Rev. E **48**, 4605 (1993).
- ²⁵F. H. Stillinger and T. A. Weber, Phys Rev A **25**, 978 (1982).
- ²⁶F. H. Stillinger and T. A. Weber, Phys. Rev. A **28**, 2408 (1983).
- ²⁷F. H. Stillinger and T. A. Weber, Science **225**, 983 (1984).
- ²⁸F. H. Stillinger and T. A. Weber, J. Phys. Chem. **87**, 2833 (1983).
- ²⁹T. A. Weber and F. H. Stillinger, J. Chem. Phys. **80**, 2742 (1984).
- ³⁰S. Sastry, P. G. Debenedetti, and F. H. Stillinger, Nature **393**, 554 (1998).
- ³¹P. G. Debenedetti and F. H. Stillinger, Nature **410**, 259 (2001).
- ³²A. Heuer, Journal of Physics: Condensed Matter **20**, 373101 (2008).
- ³³S. Sastry, Nature **409**, 164 (2001).
- ³⁴L.-M. Martinez and C. A. Angell, Nature **410**, 663 (2001).
- ³⁵G. Adam and J. H. Gibbs, The Journal of Chemical Physics **43**, 139 (1965).
- ³⁶K. Ito, C. T. Moynihan, and C. A. Angell, Nature **398**, 492 (1999).
- ³⁷I. Saika-Voivod, P. H. Poole, and F. Sciortino, Nature **412**, 514 (2001).
- ³⁸I. Saika-Voivod, F. Sciortino, and P. H. Poole, Phys. Rev. E **69**, 041503 (2004).
- ³⁹A. Saksengwijit, J. Reinisch, and A. Heuer, Phys. Rev. Lett **93**, 235701:1 (2004).
- ⁴⁰B. van Beest, G. Kramer, and R. van Santen, Phys. Rev. Lett. **64**, 1955 (1990).
- ⁴¹Z. Yu, Q. Liu, I. Szlufarska, and B. Wang, Phys. Rev. Materials **5**, 015602 (2021).
- ⁴²Z. Yu, D. Morgan, M. D. Ediger, and B. Wang, arXiv:2202.11000v1 (2022).
- ⁴³H. Tanaka, Journal of Physics: Condensed Matter **15**, L703 (2003).
- ⁴⁴R. Shi, J. Russo, and H. Tanaka, Proceedings of the National Academy of Sciences **115**, 9444 (2018).
- ⁴⁵R. Shi, J. Russo, and H. Tanaka, The Journal of Chemical Physics **149**, 224502 (2018).
- ⁴⁶A. Zeidler, P. Chirawatkul, P. S. Salmon, T. Usuki, S. Kohara, H. E. Fischer, and W. S. Howells, Journal of Non-Crystalline Solids **407**, 235 (2015), 7th IDMRCS: Relaxation in Complex Systems.
- ⁴⁷I. Petri, P. S. Salmon, and H. E. Fischer, Phys. Rev. Lett. **84**, 2413 (2000).
- ⁴⁸W. A. Crichton, M. Mezouar, T. Grande, S. Stølen, and A. Grzechnik, Nature **414**, 622 (2001).
- ⁴⁹T. G. Edwards and S. Sen, The Journal of Physical Chemistry B **115**, 4307 (2011), pMID: 21446741.
- ⁵⁰P. K. Gupta and J. C. Mauro, The Journal of Chemical Physics **130**, 094503 (2009).
- ⁵¹M. Wilson and P. S. Salmon, Phys. Rev. Lett. **103**, 157801 (2009).
- ⁵²A. C. P. Rosa Junior, C. Cruz, W. S. Santana, and M. A. Moret, Phys. Rev. E **100**, 022139 (2019).
- ⁵³A. C. P. Rosa, C. Cruz, W. S. Santana, E. Brito, and M. A. Moret, Phys. Rev. E **101**, 042131 (2020).
- ⁵⁴R. Shi and H. Tanaka, Proceedings of the National Academy of Sciences **115**, 1980 (2018).
- ⁵⁵A. Saksengwijit and A. Heuer, Phys. Rev. E **73**, 061503 (2006).
- ⁵⁶L. Lichtenstein, C. Büchner, B. Yang, S. Shaikhutdinov, M. Heyde, M. Sierka, R. Włodarczyk, J. Sauer, and H.-J. Freund, J. Angew. Chem. Int. Ed. **51**, 404 (2012).
- ⁵⁷L. Lichtenstein, M. Heyde, and H.-J. Freund, J. Phys. Chem. C **116**, 20426 (2012).
- ⁵⁸P. Y. Huang, S. Kurasch, A. Srivastava, V. Skakalova, J. Kotakoski, A. V. Krashennnikov, R. Hovden, Q. Mao, J. C. Meyer, J. Smet, D. A. Muller, and U. Kaiser, Nano Lett. **12**, 1081 (2012).
- ⁵⁹M. Heyde, S. Shaikhutdinov, and H.-J. Freund, Chem. Phys. Lett. **550**, 1 (2012).
- ⁶⁰P. K. Roy, M. Heyde, and A. Heuer, Phys. Chem. Chem. Phys. **20**, 14725 (2018).
- ⁶¹P. K. Roy and A. Heuer, Phys. Rev. Lett. **122**, 016104 (2019).
- ⁶²P. K. Roy and A. Heuer, Journal of Physics: Condensed Matter **31**, 225703 (2019).
- ⁶³S. Nosé, J. Chem. Phys. **81**, 511 (1984).
- ⁶⁴G. J. Martyna, M. L. Klein, and M. Tuckerman, The Journal of Chemical Physics **97**, 2635 (1992).
- ⁶⁵S. Büchner and A. Heuer, Phys. Rev. E **60**, 6507 (1999).
- ⁶⁶A. Heuer and S. Büchner, Journal of Physics: Condensed Matter **12**, 6535 (2000).
- ⁶⁷A. Heuer and A. Saksengwijit, Phys. Rev. E **77**, 061507 (2008).
- ⁶⁸S. Kumar, J. M. Rosenberg, D. Bouzida, R. H. Swendsen, and P. A. Kollman, Journal of Computational Chemistry **13**, 1011 (1992).
- ⁶⁹E. Gallicchio, M. Andrec, A. K. Felts, and R. M. Levy, J. Phys. Chem. B **109**, 6722 (2005).
- ⁷⁰B. Doliwa and A. Heuer, Phys. Rev. Lett. **91**, 235501 (2003).
- ⁷¹B. Doliwa and A. Heuer, Phys. Rev. E **67**, 031506 (2003).
- ⁷²F. H. Stillinger and T. A. Weber, Phys Rev B **31**, 5262 (1985).